

Spatio-Temporal Motion Retargeting for Quadruped Robots

Taerim Yoon^a, Dongho Kang^b, Seungmin Kim^a, Minsung Ahn^c,
Stelian Coros^b, Sungjoon Choi^{a,*}

^a*Department of Artificial Intelligence, Korea University, 145 Anam-ro, Seongbuk-gu,
Seoul, 02841, Korea*

^b*Department of Computer Science, ETH Zurich, Wasserwerkstrasse 12, 8092
Zürich, 8092, Switzerland*

^c*Department of Mechanical and Aerospace Engineering, University of California,
Los Angeles, 420 Westwood Plaza, Los Angeles, 90095, CA, USA*

Abstract

This work introduces a motion retargeting approach for legged robots, which aims to create motion controllers that imitate the fine behavior of animals. Our approach, namely spatio-temporal motion retargeting (STMR), guides imitation learning procedures by transferring motion from source to target, effectively bridging the morphological disparities by ensuring the feasibility of imitation on the target system. Our STMR method comprises two components: spatial motion retargeting (SMR) and temporal motion retargeting (TMR). On the one hand, SMR tackles motion retargeting at the kinematic level by generating kinematically feasible whole-body motions from keypoint trajectories. On the other hand, TMR aims to retarget motion at the dynamic level by optimizing motion in the temporal domain. We showcase the effectiveness of our method in facilitating Imitation Learning (IL) for complex animal movements through a series of simulation and hardware experiments. In these experiments, our STMR method successfully tailored complex animal motions from various media, including video captured by a hand-held camera, to fit the morphology and physical properties of the target robots. This enabled RL policy training for precise motion tracking, while baseline methods struggled with highly dynamic motion involving flying phases. Moreover, we validated that the con-

*Corresponding author

trol policy can successfully imitate six different motions in two quadruped robots with different dimensions and physical properties in real-world settings. The source code implementation of our method is publicly available at <https://terry97-guel.github.io/STMR-RL.github.io>.

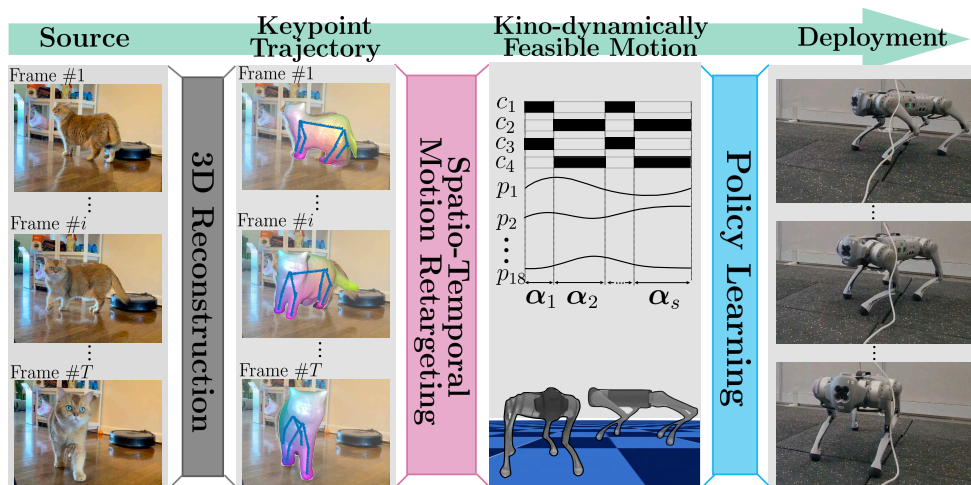
Keywords: Spatio-temporal motion retargeting; Imitation learning; Legged robots; Legged-locomotion

1. Introduction

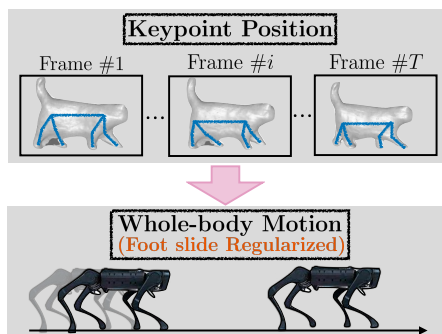
Legged robots are steadily making their way into human society for their ability to walk alongside humans. As these robots become more prevalent in everyday settings, there is increasing attention on generating natural and subtle motions beyond standard walking (Nakamura et al., 2007; Kang et al., 2021, 2022; Zhang et al., 2023b). In this context, Imitation learning (IL) (Shahbazi et al., 2016; Peng et al., 2018, 2021; Oh et al., 2023; Zhou et al., 2023; Zhang et al., 2023a; Gu and Zhu, 2024) has shown its potential to generate natural motion by imitating the prerecorded animal motions. For instance, a video showcasing a service dog carefully approaching the elderly without causing disruption can serve as a template for developing effective motion primitives for robotic assistance dogs.

The main challenge of animal motion imitation lies in overcoming the morphological and dimensional differences between source and target systems (Devin et al., 2017; Feng et al., 2023; Mayr et al., 2023). To address this issue, motion imitation involves a process known as *Motion retargeting*, which adjusts the target motion to ensure compatibility with the size and morphology of the target robotic system. (Seol et al., 2013; Villegas et al., 2018; Choi et al., 2020; Choi and Kim, 2019; Choi et al., 2021; Rouxel et al., 2022; Grandia et al., 2023).

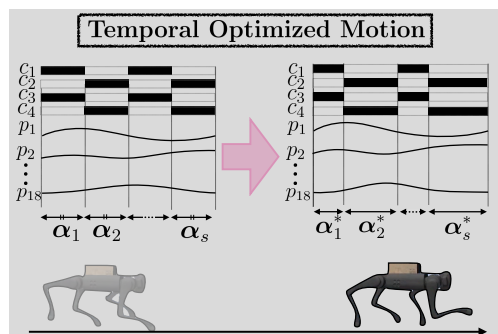
Existing motion retargeting methodologies can transfer and adapt animal motions for target systems but often produce kino-dynamically infeasible motions. These infeasible motions can result in sub-optimal mimicking behaviors or even complete failure in imitation (Levine and Koltun, 2013; Fuchioka et al., 2023; Kang et al., 2023). Additionally, the application of these methods is generally limited to motion data that includes whole-body movements with global body pose information. Consequently, this limitation restricts the use of motion data with an unknown coordinate frame, such as animal movements captured by a hand-held camera.



(a) Overview



(b) Spatial motion retargeting



(c) Temporal motion retargeting

Figure 1: (a) Our STMR method consists of SMR and TMR stages to generate kino-dynamically feasible motion. (b) In SMR stage, a kinematically feasible whole-body motion in absolute coordinates is generated, only given keypoint motion in local coordinates. (c) In TMR stage, the temporal aspect of the motion is optimized, and a dynamically feasible motion is generated. As the resulting motion is physically feasible, it can guide the training of control policy toward successful deployment in the real world.

Our work aims to generate physically feasible reference motions to facilitate streamlined and successful learning of control policies that imitate the expressiveness and agility observed in animal movements. In particular, we aim to develop a motion retargeting method that enables transferring motion data lacking global body pose information and with an unknown origin point to target robotic systems.

To this end, we propose *spatio-temporal motion retargeting* (STMR), which transfers motion with an unknown origin point to the target robot while ensuring the physical feasibility of motion imitation. Figure 1(a) illustrates two sequential processes of STMR, namely *spatial motion retargeting* (SMR) and *temporal motion retargeting* (TMR). SMR operates on a kinematic level, regulating kinematic artifacts of foot sliding and foot penetrations. Additionally, it enables the generation of whole-body motion from videos when integrated with off-the-shelf pose estimators, as depicted in Figure 1(b). On the other hand, TMR, illustrated in Figure 1(c), focuses on optimizing the temporal parameters of the motion to generate a dynamically feasible motion. This step is particularly crucial for motions that involve jumping sequences, where variations in robot size should lead to differences in mid-air duration. In the final step, a feedback control policy is trained through reinforcement learning (RL), guided by a kino-dynamically feasible reference motion to ensure accurate tracking when deployed on real robots.

To demonstrate the efficacy of our approach, we extensively experimented with six distinct motions across three robotic configurations and compared the results with three baseline methods of imitation learning. Additionally, we quantitatively show that motions generated by our STMR method are free of foot sliding and preserve contact schedules. We also showcase that STMR can generate whole-body motion by using the relative movement of keypoints and contact schedules. Finally, we demonstrate that a learned control policy can be successfully deployed in the real world on two robots with different dynamic properties and dimensions.

In summary, we propose STMR, which generates a physically feasible motion from keypoint trajectories relative to an unknown point of reference and facilitates successful imitation learning. The key contributions of our work are summarized as follows:

1. We introduce spatial and temporal motion retargeting (STMR) that transfers motion by adjusting in both spatial and temporal dimensions.
2. We present a novel approach to optimize motion in temporal dimensions by incorporating a model-based controller as an internal process.
3. We utilize residual learning to guide the training of a control policy, which is successfully deployed in the real world.

2. Related Work

Our goal is to facilitate the learning process of a control policy for quadruped robots to imitate a source motion. In accordance with this, we examine the research work focusing on studies that share similar objectives. Afterward, we turn our focus to examining existing motion retargeting methods that play crucial roles in motion imitation.

2.1. Motion imitation for quadruped robots

Developing a legged locomotion controller that can replicate legged animals' natural movements has been a longstanding aspiration. To realize this ambition, a body of research has explored the approach of incorporating prerecorded animal motion or hand-crafted motion animation into a legged locomotion control pipeline.

Several studies have demonstrated motion imitation with a model-based legged locomotion control pipeline. In the work by Kang et al. (2021), a data-driven motion planning algorithm is incorporated into the legged locomotion control pipeline. This algorithm synthesizes target gait sequences derived from a pre-recorded animal motion database, generating movements that follow high-level joystick commands. To robustly transfer the gait sequences that maintain the patterns of animal motion, both the control sequence and the footholds of robots are searched using a simplified dynamics model and a gradients-based optimization method (Kang et al., 2022). Grandia et al. (2023) developed a nested optimization technique for the retargeting of animal motion, with the goal of creating dynamically feasible target motions through the derivation of sensitivities in the retargeting parameters. They showcased the effectiveness of this method by demonstrating the retargeted motions on a quadruped robot, achieving accurate tracking through model predictive control.

In another vein, imitation learning has been a vigorously explored area of research and represents a promising strategy for imitating animal motions. Within this field, a notable contribution is the RL-based approach introduced by Peng et al. (2018). This approach formulates an RL problem using a reward function that aligns the state of a physical character with prerecorded motion data, enabling the character to perform actions such as walking, running, and dancing. This methodology was further applied to real-world robotics in later work, showcasing the execution of agile animal movements on a quadruped robot (Peng et al., 2020). More recently, an adversarial

motion prior (Peng et al., 2021) was introduced for flexible training and improved generality for inducing motion beyond the scope of the database. This approach was further extended for a quadruped robot to walk in a real-world scenario by Escontrela et al. (2022). Li et al. (2023a) took a similar approach that also utilizes adversarial imitation learning given a reference torso motion of a quadruped robot.

Rather than relying on motion data from real-world demonstrations, some studies have leveraged model-based control demonstrations to train RL policies, resulting in dynamic and agile quadruped motions. In the work of Fuchioka et al. (2023), trajectory optimization (TO) was performed offline to refine reference motion, enabling a transfer of a complex motion of quadruped backflipping. Similarly, Kang et al. (2023) introduce on-demand reference motion generation through optimal control for efficient and robust imitation learning across various quadruped gait patterns.

In this work, we utilize prerecorded animal motion data to replicate the agile and natural movement patterns observed in animals. Moreover, our approach enhances the motion imitation process by taking advantage of both model-based control and RL. Specifically, we utilize model-based control to iteratively search for kino-dynamically feasible motions. Once we obtain the refined target motions, we employ RL to train a control policy that effectively withstands external disturbance and discrepancy in modeling, which allows robots to be deployed in the real world.

2.2. Motion retargeting

In the context of motion imitation, the morphological differences between the source and target systems must be overcome to replicate motion from a system with distinct configurations. Hence, motion retargeting plays a crucial role in motion imitation as it facilitates the transfer of motions from the source to the target systems.

The most intuitive motion retargeting methods involve utilizing supervised learning with paired data between two configurations. In line with this methodology, Yamane et al. (2010) employed a Gaussian process latent model to map human motions to a character directly. Similarly, Seol et al. (2013) incorporated a technique where retargeted motion was blended with the nearest motion data point to efficiently learn the mapping from a source motion to a retargeted motion. More recently, Kim et al. (2022) used a mixture of experts trained on a paired dataset to generate real-time quadruped motions. For real-time motion retargeting in the real world, Choi et al. (2020)

constructed latent space to encompass collision-free and diverse poses. While these methods may seem straightforward, it is important to note that they often require a laborious data collection process, posing challenges in scaling the data for numerous configurations.

Another approach involves retargeting motion at the kinematic level by transferring the movement of keypoint trajectories. The work of Kwang-Jin Choi and Hyeong-Seok Ko (1999) is among the first to utilize inverse kinematics (IK) for motion retargeting by following the keypoint trajectories. Choi and Kim (2019) advanced this approach by modifying keypoint trajectories and employing IK to evaluate the deformed motion.

Building upon this foundation, the transfer of keypoint trajectories was further explored through the lens of unsupervised learning. Villegas et al. (2018) leveraged the differentiability of forward kinematics to transfer kinematic motions between human-like characters by matching the keypoint movement along with adversarial loss. Similarly, Li et al. (2023b) utilized keypoint-wise feature loss and adversarial loss to retarget humanoid motions to non-humanoid characters. A concept of the common skeleton was also introduced to construct intermediate latent space shared among different kinematic structures using unsupervised learning (Aberman et al., 2020). Choi et al. (2021) proposed a self-supervised learning framework to ensure a safe motion retargeting process, wherein pseudo-labels were acquired through optimization-based motion retargeting approaches.

While the kinematic motion retargeting methods mentioned previously can generate visually convincing motions, incorporating dynamic properties can significantly aid in achieving physically feasible motions and deploying robots in the real world. Tak and Ko (2005) introduced a dynamic motion retargeting filter for legged figures. This method applies Zero-Moment Point (ZMP) constraints to enable dynamically stable walking. Similarly, Al Borno et al. (2018) employed linear quadratic regulator (LQR) search trees to track keypoint trajectories of the source motion (Al Borno et al., 2018). Rouxel et al. (2022) utilized whole-body optimization of kino-dynamics to retarget motion involving multi-contacts. The research by Grandia et al. (2023) can also be classified under this dynamic motion retargeting approach since it considers the dynamics of the target system during the motion retargeting process.

In this paper, we account for both kinematics and dynamics to retarget motions to generate physically feasible motions. In particular, our method prevents kinematics artifacts (e.g., foot sliding) while preserving the contact

schedules to maintain the semantic meaning of the motion. Moreover, we retarget a motion between robots with significantly different dynamic properties by refining the motion in the temporal dimension.

3. Preliminaries

This section describes two established methods, each for retargeting a motion at kinematic and dynamic levels. As our proposed method produces physically feasible movements by sequentially refining a target motion at kinematic and dynamic levels, we leverage these existing techniques as sub-processes. To be specific, we utilize the unit vector method (UV) (Choi and Kim, 2019) for kinematic motion retargeting and Differential Dynamic Programming (DDP) (Mayne, 1973) for dynamic motion retargeting.

3.1. Unit Vector method

The unit vector method retargets a motion by preserving the directional unit vector between two adjacent keypoints. We note that the motion obtained by this method can be kinematically infeasible. However, we can use it as a reference for generating a physically feasible whole-body motion.

Consider a robot whose joint position is denoted as $\boldsymbol{\theta} \in \mathbb{R}^M$ and keypoint position as $\mathbf{p} \in \mathbb{R}^{N \times 3}$, where M and N are the numbers of joints and keypoints, respectively. The unit vector method aims to obtain joint position $\boldsymbol{\theta}$ given the keypoint positions of the source system, denoted as ${}^{\text{src}}\mathbf{p}$.

Initially, it generates a keypoint position of the target system, denoted as ${}^{\text{trg}}\mathbf{p}$ by scaling the directional vector obtained from the keypoint position of the source system ${}^{\text{src}}\mathbf{p}$. Let us define an indexing function $\mathcal{P}(\cdot)$ that maps the keypoint index to its parent index of the kinematic tree. The unit directional vector between j th keypoint and its parent can be described as $\mathbf{e}_j = (\mathbf{p}_j - \mathbf{p}_{\mathcal{P}(j)})/d_j$ where $d_j := \|\mathbf{p}_j - \mathbf{p}_{\mathcal{P}(j)}\|$ is constant as two keypoints lies on rigid link. To preserve the unit directional vector of the source and target system, the keypoint position of the target system is obtained by scaling ${}^{\text{src}}\mathbf{e}_j$ with ${}^{\text{trg}}d_j$ as

$${}^{\text{trg}}\mathbf{p}_j = {}^{\text{trg}}\mathbf{p}_{\mathcal{P}(j)} + {}^{\text{trg}}d_j {}^{\text{src}}\mathbf{e}_j. \quad (1)$$

Subsequently, the joint position $\boldsymbol{\theta}$ is obtained by solving inverse kinematics.

$$\boldsymbol{\theta} = \mathbf{IK}({}^{\text{trg}}\mathbf{p}_{1:N})$$

3.2. Differential Dynamic Programming

Model-based optimal control (MBOC) is a widely adopted approach for motion control. Among the various strategies employed in MBOC, Differential Dynamic Programming (DDP) stands out for its capacity to integrate complex system dynamics models to search for optimal control sequences. Given that our proposed method encompasses dynamic motion retargeting, DDP is utilized as an internal process. Specifically, we utilize an Iterative Linear Quadratic Gaussian (ILQG) (Tassa et al., 2012), a variant of Differential Dynamic Programming (DDP).

Let us denote the dynamics of the robot by f , where the discrete-time dynamics at i th frame can be described as

$$\mathbf{x}^{i+1} = f(\mathbf{x}^i, \mathbf{u}^i). \quad (2)$$

The goal of DDP is to track the target states, denoted as $\bar{\mathbf{X}}$, subject to the dynamics f , which can be represented as Equation 3. As in Equation 3, we minimize the objective function, denoted as \mathcal{J} , comprising the sum of the running cost l and the final cost l_f , where $*$ indicates optimized values.

$$\begin{aligned} \min_{\mathbf{U}} \quad \mathcal{J} &:= \sum_{i=0}^{h-1} l(\mathbf{x}^i, \mathbf{u}^i; \bar{\mathbf{x}}^i) + l_f({}^h\mathbf{x}; {}^h\bar{\mathbf{x}}) \\ \text{s.t.} \quad \mathbf{x}^{i+1} &= f(\mathbf{x}^i, \mathbf{u}^i). \end{aligned} \quad (3)$$

Denoting the value function at i th step as $V(\mathbf{x}) = \mathcal{J}(\mathbf{x}, {}^i\mathbf{u}^*)$ and at the next step as V' , Bellman optimality principle can be written as

$$V(\mathbf{x}) = \min_{\mathbf{u}} [l(\mathbf{x}, \mathbf{u}) + V'(f(\mathbf{x}, \mathbf{u}))]. \quad (4)$$

Furthermore, perturbing around state-action pair (\mathbf{x}, \mathbf{u}) on Equation 4 can be written as

$$\begin{aligned} Q(\delta\mathbf{x}, \delta\mathbf{u}) &= l_i(\mathbf{x} + \delta\mathbf{x}, \mathbf{u} + \delta\mathbf{u}) - l_i(\mathbf{x}, \mathbf{u}) \\ &\quad + V'(f(\mathbf{x} + \delta\mathbf{x}, \mathbf{u} + \delta\mathbf{u})) - V'(f(\mathbf{x}, \mathbf{u})). \end{aligned} \quad (5)$$

Then, we expand Q with second-order approximation with the coefficients

$$Q_{\mathbf{x}} = l_{\mathbf{x}} + f_{\mathbf{x}}^T V'_{\mathbf{x}} \quad (6a)$$

$$Q_{\mathbf{u}} = l_{\mathbf{u}} + f_{\mathbf{u}}^T V'_{\mathbf{x}} \quad (6b)$$

$$Q_{\mathbf{xx}} = l_{\mathbf{xx}} + f_{\mathbf{x}}^T V'_{\mathbf{xx}} f_{\mathbf{x}} + V'_{\mathbf{x}} \cdot f_{\mathbf{xx}} \quad (6c)$$

$$Q_{\mathbf{uu}} = l_{\mathbf{uu}} + f_{\mathbf{u}}^T V'_{\mathbf{uu}} f_{\mathbf{u}} + V'_{\mathbf{x}} \cdot f_{\mathbf{uu}} \quad (6d)$$

$$Q_{\mathbf{ux}} = l_{\mathbf{ux}} + f_{\mathbf{u}}^T V'_{\mathbf{xx}} f_{\mathbf{x}} + V'_{\mathbf{x}} \cdot f_{\mathbf{ux}}. \quad (6e)$$

From second-order expansion, the optimal control modification $\delta \mathbf{u}^*$ is obtained as

$$\delta \mathbf{u}^* = -Q_{\mathbf{uu}}^{-1}(Q_{\mathbf{u}} + Q_{\mathbf{ux}} \delta \mathbf{x}). \quad (7)$$

By ignoring the second order derivative of dynamics (i.e. $f_{\mathbf{xx}}, f_{\mathbf{uu}}, f_{\mathbf{ux}}$), each coefficient can be recursively obtained as

$$\Delta V(i) = -\frac{1}{2} Q_{\mathbf{u}} Q_{\mathbf{uu}}^{-1} Q_{\mathbf{u}} \quad (8a)$$

$$V_{\mathbf{x}}(i) = Q_{\mathbf{x}} - Q_{\mathbf{u}} Q_{\mathbf{uu}}^{-1} Q_{\mathbf{ux}} \quad (8b)$$

$$V_{\mathbf{xx}}(i) = Q_{\mathbf{xx}} - Q_{\mathbf{xu}} Q_{\mathbf{uu}}^{-1} Q_{\mathbf{ux}}. \quad (8c)$$

4. Problem Formulation

In this section, we introduce essential notations and formulate the spatio-temporal motion retargeting (STMR) problem. In the latter part of this section, we make the STMR problem tractable by decoupling it into a two-stage problem of spatial and temporal motion retargeting.

4.1. Notations

Consider a robot with M joints whose joint position is denoted as $\boldsymbol{\theta} \in \mathbb{R}^M$. The base position of the robot is denoted as $\mathbf{p}_b \in \mathbb{R}^3$, and base orientation represented with quaternion is denoted as $\mathbf{h} \in \mathbb{H}$ where \mathbb{H} is unit quaternion space. The generalized coordinate of the robot is defined by stacking these values denoted as $\mathbf{q} = [\mathbf{p}_b \ \mathbf{h} \ \boldsymbol{\theta}]^T$. Similarly, we denote linear, angular, joint velocity as $\mathbf{v} \in \mathbb{R}^3, \mathbf{w} \in \mathbb{R}^3$, and $\dot{\boldsymbol{\theta}} \in \mathbb{R}^M$, respectively. The time derivative of generalized coordinate is accordingly defined as $\dot{\mathbf{q}} = [\mathbf{v}, \mathbf{w}, \dot{\boldsymbol{\theta}}]$ and the state of the robot is defined as $\mathbf{x} = [\mathbf{q}, \dot{\mathbf{q}}]^T$.

Additionally, we denote the keypoint position as $\mathbf{p} \in \mathbb{R}^{N \times 3}$, where N is the number of keypoints. Specifically, we focus on $N = 16$ keypoints consisting of four hips, thighs, knees, and feet.

These values are specified for each frame, with the maximum frame index denoted by T . For instance, the position of the j th keypoint in the i th frame is denoted as \mathbf{p}_j^i , where $j \in [1, 2, \dots, N]$ and $i \in [0, 1, 2, \dots, T]$.

4.2. Spatio-temporal motion retargeting

As keypoint trajectory $\mathbf{p}_{1:N}^{0:T}$ is acquired from an arbitrary quadruped system, it can be physically infeasible for the target robot to track. Furthermore, the keypoint trajectory $\mathbf{p}_{1:N}^{0:T}$ does not contain the base movement required for whole-body imitation. Therefore, STMR regenerates the physically feasible whole-body motion by optimizing spatial and temporal dimensions.

Let us define the temporal parameters as $\boldsymbol{\alpha}$ that deforms motion by scaling in the time domain. The objective of the STMR (Spatio-Temporal Motion Retargeting) problem is to establish a mapping $\mathbf{ST}_{\boldsymbol{\alpha}} : \mathbf{p}_{1:N}^{0:T} \rightarrow \mathbf{X}^*$, aiming to produce robot states \mathbf{X}^* that are both kinematically and dynamically feasible. We approach this as a numerical optimization problem, where, given the discrete dynamics f , we aim to find the optimal temporal parameters $\boldsymbol{\alpha}^*$ and control sequence \mathbf{U}^* , as described in Equation 9. The search incorporates additional constraints, notably foot constraints g , to ensure the motion remains kinematically feasible. The predefined search ranges of temporal parameters $\boldsymbol{\alpha}$ are denoted as \mathcal{I} .

$$\begin{aligned}
\min_{\mathbf{U}, \boldsymbol{\alpha}} \quad & \mathcal{J} := \sum_{i=0}^{T-1} l(\mathbf{x}^i, \mathbf{u}^i, \mathbf{ST}_{\boldsymbol{\alpha}}^i(\mathbf{p}_{1:N}^{0:T})) + l_f(\mathbf{x}^T, \mathbf{ST}_{\boldsymbol{\alpha}}^T(\mathbf{p}_{1:N}^{0:T})) \\
\text{s.t.} \quad & g(\mathbf{X}) = 0, \\
& \mathbf{x}^{i+1} = f(\mathbf{x}^i, \mathbf{u}^i), \\
& \boldsymbol{\alpha} \in \mathcal{I}.
\end{aligned} \tag{9}$$

It is worth noting that the STMR problem involves actively deforming the target motion rather than mere tracking. Therefore, the motion retargeting function $\mathbf{ST}_{\boldsymbol{\alpha}}(\cdot)$ should be constructed in a way that its resulting motion does not lose the semantic meaning of the original motion. We preserve the overall expressiveness of the motion by deforming in temporal dimensions. Additionally, due to its nonconvex nature, the standard convex optimization methodologies can not be applied. To address this, we divide this problem into two subproblems: spatial motion retargeting (SMR) and temporal motion retargeting (TMR).

4.3. Spatio-Temporal decoupling

Due to the challenges mentioned earlier, we decompose the STMR problem as $\mathbf{ST}_\alpha(\cdot) = \mathbf{T}_\alpha \circ \mathbf{S}(\cdot)$ where $\mathbf{S}(\cdot)$ represents SMR, and $\mathbf{T}_\alpha(\cdot)$ represents TMR process. Adopting this approach, we find these two mappings sequentially through two-stage optimization.

The SMR maps keypoint trajectory $\mathbf{p}_{1:N}^{0:T}$ to kinematically feasible robot states, denoted as $\bar{\mathbf{X}}$ such that $\mathbf{S} : \mathbf{p}_{1:N}^{0:T} \rightarrow \bar{\mathbf{X}}$. Specifically, we enforce kinematic feasibility with foot constraints g . Since we focus on kinematic motion, the dynamics f is dropped, and the state-only objective function denoted as \mathcal{J}_x is minimized under foot constraints g , as shown in Equation 10.

$$\bar{\mathbf{X}} = \arg \min_{\mathbf{X}} \mathcal{J}_x \quad \text{s.t.} \quad g(\mathbf{X}) = 0 \quad (10)$$

Following this, a temporal retargeting function, denoted as $\mathbf{T}_\alpha(\cdot)$, obtains dynamically feasible states \mathbf{X}^* such that $\mathbf{T}_\alpha : \bar{\mathbf{X}} \rightarrow \mathbf{X}^*$. In particular, \mathbf{T}_α performs temporal deformation by dividing the motion into S segments with an equal time step size and scaling each with temporal parameters α that lies in interval $\mathcal{I} = [\alpha_{\min}, \alpha_{\max}]$ for $\alpha_{\min}, \alpha_{\max} \in \mathbb{R}_{>0}^S$. In detail, TMR solves the optimization problem from Equation 9 where the objective function is written as Equation 11.

$$\mathcal{J} = \sum_{i=0}^{T-1} l(\mathbf{x}^i, \mathbf{u}^i, \mathbf{T}_\alpha^i(\bar{\mathbf{X}})) + l_f(\mathbf{x}^T, \mathbf{T}_\alpha^T(\bar{\mathbf{X}})) \quad (11)$$

The TMR problem encompasses a finite-horizon optimal control problem (OCP), which aims to find the optimal control sequence to track the given reference states under dynamics. For example, by ignoring the temporal parameter α , the TMR problem reduces to OCP with the goal of tracking the reference states $\bar{\mathbf{X}}$. This property allows us to utilize model-based optimal control (MBOC) (Tassa et al., 2012) as a subprocess of TMR to solve for control sequence \mathbf{U}^* .

5. Methods

In this section, we outline the methodology for solving STMR problem, encompassing two distinct sub-problems: spatial motion retargeting (SMR) and temporal motion retargeting (TMR). Furthermore, we detail the residual policy learning procedures for executing retargeted motions on robots.

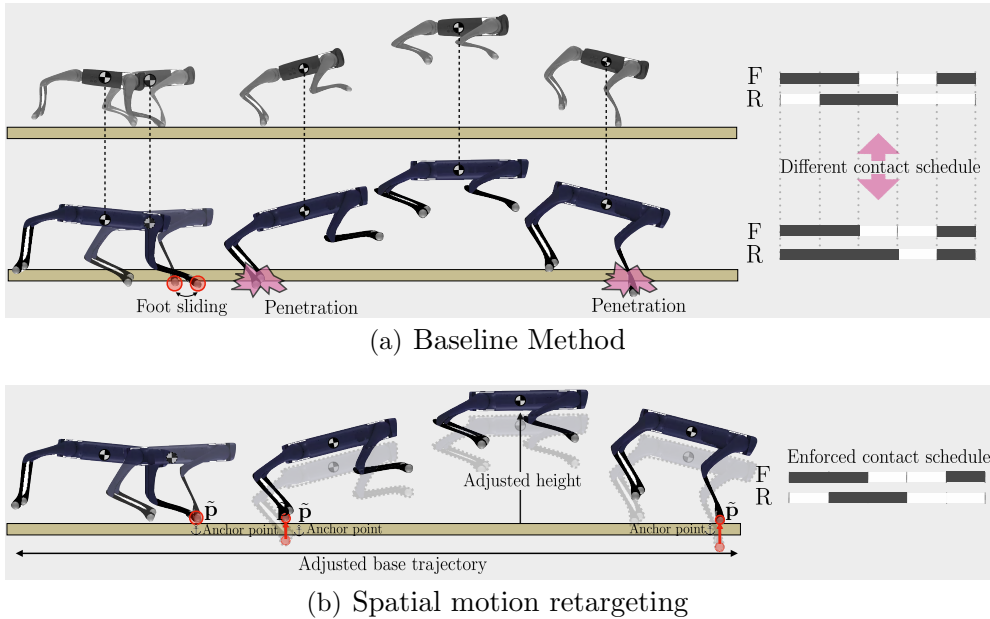


Figure 2: Illustration of baseline method and spatial motion retargeting (SMR). (a) The baseline method (i.e., unit vector method) can lead to kinematic artifacts such as foot sliding, foot penetration, and mismatched contact timing. (B) On the other hand, SMR generates kinematically feasible motion by appropriately anchoring the foot position as $\hat{\mathbf{p}}$.

5.1. Spatial Motion Retargeting

The unit-vector method, as outlined in Section 3.1, retargets motion on a kinematic level, maintaining the directional unit vector between adjacent keypoints. However, this approach may introduce undesired artifacts like foot sliding and foot penetration. For instance, Figure 2(a) illustrates that transferring a walking trajectory by a short-legged robot (above) to the long-legged robot (below) leads to unnatural foot sliding and penetration. Additionally, the unit-vector method can not generate the base trajectory other than direct transfer, unable to adjust the base trajectory to the kinematic configuration. More critically, the naive transfer using the unit-vector method can also change contact schedules, which fails to mimic the subtle gestures of the original motion.

To address these issues, we propose a spatial motion retargeting method, illustrated in Figure 2(b), that eliminates foot sliding and foot penetration, adjusts base trajectory and heights according to kinematic morphology, and preserves contact schedules. More specifically, we introduce two constraints:

Algorithm 1 Spatial Motion Retargeting

```
1: function UPDATEANCHOR( $\tilde{\mathbf{p}}, \mathbf{q}, \mathbf{c}, i$ )
2:   for  $j = 1$  to 4 do
3:     if  $\mathbf{c}_j^i$  and not  $\mathbf{c}_j^{i-1}$  then ▷ At the new contact segment
4:        $\tilde{\mathbf{p}}_j \leftarrow \text{PROJECTGROUND}(\mathbf{FK}_j(\mathbf{q}))$ 
5:     end if
6:   end for
7:   return  $\tilde{\mathbf{p}}$ 
8: end function
9: function SPATIALMOTIONRETARGETING( ${}^{UV}\mathbf{q}$ )
10:   $\mathbf{q}^0 \leftarrow {}^{UV}\mathbf{q}^0$ 
11:   $\tilde{\mathbf{p}} \leftarrow \text{PROJECTGROUND}(\mathbf{FK}(\mathbf{q}))$ 
12:   ${}^{UV}\dot{\mathbf{q}} \leftarrow \text{DIFFERENTIATE}({}^{UV}\mathbf{q}, 0)$ 
13:  for  $i = 1$  to  $N$  do
14:    if ANY( $\mathbf{c}^i$ ) then
15:       ${}^{UV}\dot{\mathbf{q}} \leftarrow \text{DIFFERENTIATE}({}^{UV}\mathbf{q}^i, {}^{UV}\mathbf{q}^{i+1}, \Delta t)$ 
16:    else
17:       ${}^{UV}\dot{\mathbf{q}} \leftarrow \text{INTEGRATE}({}^{UV}\dot{\mathbf{q}}, \mathbf{g}, \Delta t)$ 
18:    end if
19:     $\bar{\mathbf{q}} \leftarrow \text{INTEGRATE}(\mathbf{q}^{i-1}, {}^{UV}\dot{\mathbf{q}}, \Delta t)$ 
20:    while True do
21:       $\mathbf{J} \leftarrow \text{GETJACOBIAN}(\mathbf{q})$ 
22:       $\dot{\mathbf{q}} \leftarrow (\mathbf{J}\mathbf{J}^T + \lambda\mathbf{I})\mathbf{J}^T[\mathbf{c}(\tilde{\mathbf{p}} - \mathbf{FK}(\mathbf{q})) - \mathbf{JK}(\mathbf{q}^i - \bar{\mathbf{q}})]$ 
23:      if  $\dot{\mathbf{q}} < \dot{\mathbf{q}}_{\text{thres}}$  then
24:        break
25:      end if
26:       $\mathbf{q}^i \leftarrow \mathbf{q}^i + \eta\dot{\mathbf{q}}$ 
27:    end while
28:     $\tilde{\mathbf{p}} \leftarrow \text{UPDATEANCHOR}(\tilde{\mathbf{p}}, \mathbf{q}^i, \mathbf{c}, i + 1)$ 
29:  end for
30:  return  $\mathbf{q}$ 
31: end function
```

the *contact preservation constraint*, which ensures that the contact schedule of the source and retargeted motion remains identical without any foot penetration, and the *foot locking constraint*, which prevents foot sliding during the contact phase. Under these constraints, SMR aims to obtain a refined state of robot $\bar{\mathbf{X}}$ that mimics the original motion as described in the following sections.

5.1.1. Foot Regularizing Constraints

We denote forward kinematics as \mathbf{FK} which maps \mathbf{q} to the global position of j th foot represented as $\mathbf{FK}_j(\mathbf{q})$, where $j \in \{1, 2, 3, 4\}$. Additionally, we introduce the anchor position of j th foot as $\tilde{\mathbf{p}}_j$, which is a projection of $\mathbf{FK}_j(\mathbf{q})$ to the ground. We also denote the jacobian of forward kinematics as $\mathbf{J}_j = \frac{\partial(\mathbf{FK}_j(\mathbf{q}))}{\partial\mathbf{q}} \in \mathbb{R}^{(M+6) \times 3}$.

To satisfy the contact preservation constraint, the height of the foot should match the elevation of the projection point during contact and should be positioned above this point when not in contact, as

$$\begin{cases} \mathbf{FK}_j(\mathbf{q})^z = \tilde{\mathbf{p}}_j^z, & \text{if } c_j \\ \mathbf{FK}_j(\mathbf{q})^z > \tilde{\mathbf{p}}_j^z, & \text{else,} \end{cases} \quad (12)$$

where z represents the height component of the position vector, and c_j is a contact boolean for j th foot.

To enforce the foot locking constraint, we fix the foot position to the anchor point whose position $\tilde{\mathbf{p}}_j$ is updated for the new contact segment.

$$\mathbf{FK}_j(\mathbf{q})^{xy} = \tilde{\mathbf{p}}_j^{xy} \quad \text{if } c_j \quad (13)$$

Equation 12 and Equation 13 are then combined and relaxed as follows:

$$c_j(\mathbf{FK}_j(\mathbf{q}) - \tilde{\mathbf{p}}_j) = 0 \quad (14)$$

5.1.2. Mimicing Objective

Let us denote the coordinates obtained by the unit vector methods as ${}^{\text{UV}}\mathbf{q}$ and its time derivative as ${}^{\text{UV}}\dot{\mathbf{q}}$. The reference coordinate is defined as $\bar{\mathbf{q}}$, which is obtained by time-integrating the current coordinate \mathbf{q} with ${}^{\text{UV}}\dot{\mathbf{q}}$. Additionally, the scaled error between reference coordinates $\bar{\mathbf{q}}$ and current coordinate \mathbf{q} is denoted as $\delta\bar{\mathbf{q}} = K(\bar{\mathbf{q}} - \mathbf{q})$, where K is controller gain.

We search for the generalized coordinate \mathbf{q} by solving the optimization problem specified in Equation 15, where the objective is to mimic the reference $\bar{\mathbf{q}}$ under linearized constraints from Equation 14.

$$\begin{aligned} \dot{\mathbf{q}} = \arg \min_{\dot{\mathbf{q}}} & \frac{1}{2}(\dot{\mathbf{q}} - \delta\bar{\mathbf{q}})^T \mathbf{Q}(\dot{\mathbf{q}} - \delta\bar{\mathbf{q}}) \\ \text{s.t. } & \mathbf{J}_j \dot{\mathbf{q}} = c_j(\tilde{\mathbf{p}}_j - \mathbf{FK}_j(\mathbf{q})), \quad j \in [1, 2, 3, 4] \end{aligned} \quad (15)$$

Applying Levenberg-Marquardt Algorithm (Chiaverini et al., 1994), we soften the constraints and solve the optimization problem as Equation 16,

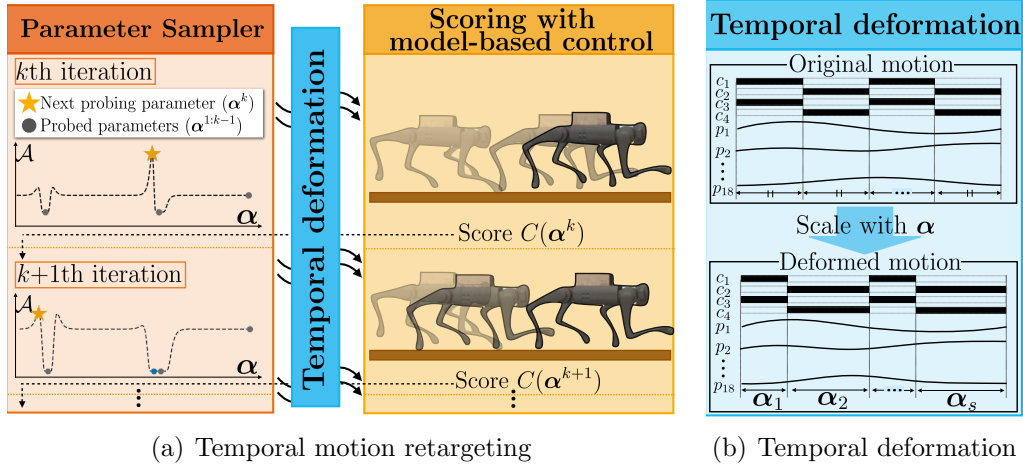


Figure 3: (a) The overview of temporal motion retargeting (TMR) is illustrated. Using acquisition function \mathcal{A} , the temporal parameter α is sampled for temporal deformation and scored by model-based control. (b) Temporal deformation involves splitting the motion into equal segments and scaling with temporal parameter α .

where the dropped index of j indicates row-wise stacking and λ denotes a damping factor.

$$\dot{\mathbf{q}} = (\mathbf{J}\mathbf{J}^T + \lambda\mathbf{I})\mathbf{J}^T[\mathbf{c}(\tilde{\mathbf{p}}_{1:4}) - \mathbf{F}\mathbf{K}_{1:4}(\mathbf{q})] - \mathbf{J}\delta\tilde{\mathbf{q}} \quad (16)$$

Finally, the kinematically feasible states $\bar{\mathbf{X}}$ can be obtained by stacking the obtained \mathbf{q} and $\dot{\mathbf{q}}$. The overall algorithm of spatial motion retargeting is summarized in Algorithm 1.

5.2. Temporal Motion Retargeting

In the TMR stage, we generate dynamically feasible motions for the target robot by determining the temporal parameters α and control sequence \mathbf{U} , as outlined in Section 4.2. The concurrent optimization of both α and \mathbf{U} poses significant challenges. Therefore, instead of tackling the joint optimization problem, we employ the MBOC approach described in Section 3.2 to compute the control sequence \mathbf{U} for a specified α and score the motion deformed by temporal parameter. We then iteratively search for the optimal temporal parameters α^* using Bayesian Optimization and (BO) (Snoek et al., 2012a).

Figure 3(a) illustrates the procedures of TMR. As illustrated on the left side of Figure 3(a), we initially sample the temporal parameter; for

the first iteration, this sampling is performed randomly within the interval $\mathcal{I} = [\boldsymbol{\alpha}_{\min}, \boldsymbol{\alpha}_{\max}]$. Then, the motion is deformed in the temporal dimension according to temporal parameter $\boldsymbol{\alpha}$, as shown in Figure 3(b). The deformed motion is tracked by MBOC and evaluated with the scoring function $C(\cdot)$. Finally, the next temporal parameter $\boldsymbol{\alpha}$ for evaluation is selected based on the pairwise relationship between $\boldsymbol{\alpha}$ and $C(\cdot)$. We repeat the entire process until we identify an $\boldsymbol{\alpha}$ that achieves a convergence. Each step of this process is elaborated further in the subsequent sections.

5.2.1. Temporal deformation

We deform the states $\bar{\mathbf{X}}$ using the temporal retargeting function $\mathbf{T}(\cdot)$. As illustrated in Figure 3(b), the source motion is divided into n_s equal intervals. We then obtain the temporally deformed motion $\mathbf{S}(\bar{\mathbf{X}})$ by scaling each interval with $\boldsymbol{\alpha}$. Notably, the temporal deformation of the robot’s state $\bar{\mathbf{X}}$ affects the joint-wise movements and the contact schedules.

5.2.2. Scoring with Model-based Control

We employ MBOC to evaluate the trajectory deformed by the temporal parameter $\boldsymbol{\alpha}$. The underlying intuition is that appropriately deformed motion will result in better tracking performance by MBOC. Equation 17 shows the control performance, $C(\boldsymbol{\alpha})$, includes measuring contact differences via Intersection over Union (IoU), base positional error (L1 distance d_b), and base orientation error (L1 distance of Euler angles d_E). Notably, the positional error of keypoints is excluded for simplicity, as tracking keypoint motion is relatively straightforward for MBOC.

$$C(\boldsymbol{\alpha}) = d_b(\mathbf{p}_b, \bar{\mathbf{p}}_b) + d_E(\mathbf{h}_b, \bar{\mathbf{h}}_b) + w_c \text{IoU}(\mathbf{c}, \bar{\mathbf{c}}) + w_\alpha \|\boldsymbol{\alpha}\| \quad (17)$$

5.2.3. Parameter Sampling

Denoting the temporal parameter at k th iteration as $\boldsymbol{\alpha}^k$ and its score as C^k , our goal is to sample the next probing parameter $\boldsymbol{\alpha}^{k+1}$ based on the previous probing points $(\boldsymbol{\alpha}^{1:k}, C^{1:k})$. We first fit the surrogate function s , using the Gaussian process regression with a Matern kernel $\mathbf{K}(\cdot, \cdot)$:

$$\begin{aligned} s(\boldsymbol{\alpha}) &\sim \mathcal{GP}(s_\mu(\boldsymbol{\alpha}), \mathbf{K}(\boldsymbol{\alpha}, \boldsymbol{\alpha}')), \\ s_\mu &= \mathbf{K}_*^T \mathbf{K}^{-1} C^{1:k-1}, \quad s_\sigma = \mathbf{K}_{**} - \mathbf{K}_*^T \mathbf{K} \mathbf{K}_*, \end{aligned} \quad (18)$$

where $\mathbf{K} = \mathbf{K}(\boldsymbol{\alpha}^{1:k}, \boldsymbol{\alpha}^{1:k})$, $\mathbf{K}_* = \mathbf{K}(\boldsymbol{\alpha}, \boldsymbol{\alpha}^{1:k})$, $\mathbf{K}_{**} = \mathbf{K}(\boldsymbol{\alpha}, \boldsymbol{\alpha})$.

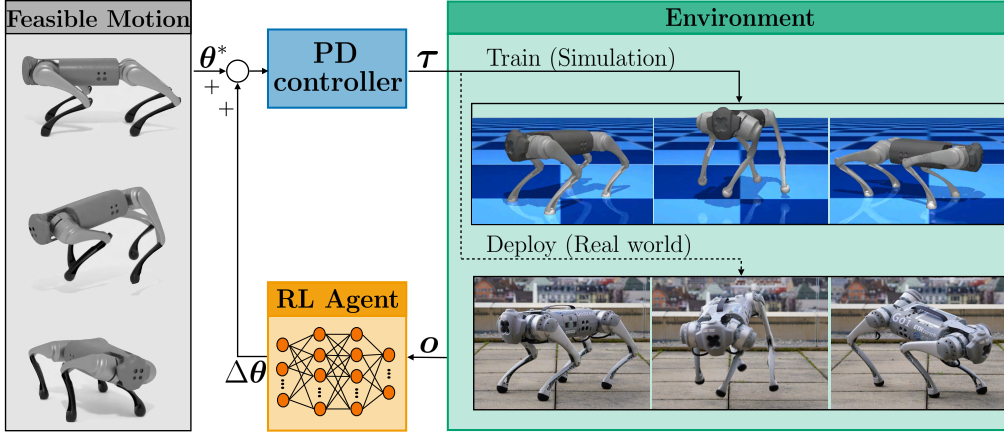


Figure 4: Control policy with residual learning

Then, we construct an acquisition function \mathcal{A} with Expected Improvement (EI) (Snoek et al., 2012b), where $\hat{\alpha}$ is the best parameter so far, ϕ denotes Gaussian distribution, Φ is cumulative distribution function (CDF) of ϕ , and ξ controls the degree of exploration.

$$\begin{aligned} \mathcal{A} &= \Delta s \Phi(\Delta s / s_\sigma) + s_\sigma \phi(\Delta s / s_\sigma) \\ \Delta s &= s_\mu(\alpha) - s_\mu(\hat{\alpha}) + \xi, \quad \hat{\alpha} = \max(\alpha^{1:k}). \end{aligned} \quad (19)$$

Finally, we sample the next probing parameter α^l that maximizes the acquisition function as described in Equation 20.

$$\alpha^{k+1} = \arg \max_{\alpha} \mathcal{A}(\alpha) \quad (20)$$

5.3. Residual policy learning

As a final step, we adopt residual policy learning (Johannink et al., 2019) to guide the feedback policy learning process by leveraging the kinodynamically feasible motion. More specifically, we train a residual policy π to serve as a closed-loop control where the motion \mathbf{X}^* obtained through STMR serves as a base control signal. As illustrated in Figure 4, the joint values of feasible motion θ^* are obtained directly from indexing the feasible motion \mathbf{X}^* where the residual control policy outputs the joint correction denoted as $\Delta\theta$. Both terms are fed to the PD controller to yield a motor torque command as $\tau = K_p(\theta^* + \Delta\theta - \theta) - K_d\dot{\theta}$, where K_p and K_d are the proportional and derivative gains, respectively.

The residual policy is trained with RL, where the rewards at frame i are defined as a summation of tracking measures for joint position $\boldsymbol{\theta}_{1:M}^i$, base position \mathbf{q}_b^i , base orientation \mathbf{h}^i , the position of key points $\mathbf{p}_{1:N}^i$ as follows:

$$r_t^i = w_q \exp[\beta_q \|\bar{\boldsymbol{\theta}}_{1:M}^i - \boldsymbol{\theta}_{1:M}^i\|] + w_b \exp[\beta_b \|\bar{\mathbf{p}}_b^i - \mathbf{p}_b^i\|] + w_h \exp[\beta_h \|\bar{\mathbf{h}}^i \ominus \mathbf{h}^i\|] + w_p \exp[\beta_p \|\bar{\mathbf{p}}_{1:N}^i - \mathbf{p}_{1:N}^i\|]. \quad (21)$$

The observation space, denoted as \mathbf{o} , is defined in Equation 22 which consists of projected gravity \mathbf{g}_{proj} , joint positions $\boldsymbol{\theta}$, joint velocity $\dot{\boldsymbol{\theta}}$, last deployed torque $\boldsymbol{\tau}$, phase variable ϕ , and base height \mathbf{p}_b^z :

$$\mathbf{o} = [\mathbf{g}_{\text{proj}}, \boldsymbol{\theta}, \dot{\boldsymbol{\theta}}, \boldsymbol{\tau}, \phi, \mathbf{p}_b^z]. \quad (22)$$

6. Simulational Experiments

We conducted a series of simulation experiments to show the efficacy of the proposed method. In these experiments, we evaluated the motion tracking performance of the motion control policies using the retargeted motions from our STMR method and compared the results against the ones with baseline imitation learning methodologies. We also validated that the motion transferred by our method is free of foot sliding and preserves the contact schedules. Additionally, we demonstrated the reconstruction of base movements from baseless motions captured using a hand-held camera.

6.1. Training details

The control policies are trained on a legged gym (Smith et al., 2022) that utilizes Isaac Gym (Makoviychuk et al., 2021) for massively parallel simulations. Each experiment utilized Proximal Policy Optimization (PPO) (Schulman et al., 2017) with 10,000 iterations, equivalent to approximately 50 million data samples requiring one hour of training with a GPU (RTX A6000, Nvidia). Each of the comparing methods is trained using 5 randomized seeds, where we report the metric in terms of their mean and standard deviation. More details on training configuration are summarized in Table 1.

6.2. Baselines

To compare the motion tracking performance, we set three imitation learning methods as baselines. In particular, the baselines are selected to show the effect of guided policy learning with motions optimized in space and time dimensions.

Hidden dimensions (Actor)	[512, 256, 128]
Hidden dimensions (Critic)	[512, 256, 128]
Activation function	Exponential Linear Unit (ELU)
Weight coefficient for Entropy term	0.01
Learning rate	1.0e-3
Discount factor	0.99
Optimizer	ADAM (Kingma and Ba, 2014)
Number of policy iterations	10,000
Number of policy iterations (AMP)	25,000

Table 1: Training configuration for baseline methods.

6.2.1. *DeepMimic*

We set DeepMimic (Peng et al., 2018) as baselines to evaluate the impact of kino-dynamically feasible motion. The reference motion is obtained using the unit vector method, and the base position is transferred directly. The reward term mirrors Equation 21, whereas the initial state is determined through uniform sampling from the reference, namely the reference state initialization scheme.

6.2.2. *Adversarial Motion Prior*

The AMP (Escontrela et al., 2022) approach can circumvent the requirement for dynamic feasible reference motions to some extent. This is possible by using a reward derived from a learned discriminator that helps the agent in learning smooth transitions between states that mimic the patterns of prior motion data. We compare our proposed method with AMP to highlight the importance of taking into account the physical feasibility of reference motions for motion imitation.

More specifically, we train a discriminator D to classify whether the transition between the current state s and the next state s' is generated by the agent or from a reference motion. The output from the discriminator D contributes an additional reward term with the corresponding weight w_{ad} as

$$r = r_t + w_{\text{ad}} \log D(s, s'). \quad (23)$$

For the AMP policy, the training iterations were extended to 25,000 to achieve convergence as shown in Table 1.

6.2.3. *OptMimic*

Our method is similar to OptMimic (Fuchioka et al., 2023), where the dense description of dynamic motion is obtained to improve control policy

Motion	Robot	DeepMimic	AMP	OptMimic	STMR (ours)
Trot0	Go1	109.8(76.7)	422.4(297.8)	69.1(17.3)	59.0(23.5)
	A1	104.9(44.6)	120.3(17.5)	40.1(4.3)	54.6(8.9)
	AlienGo	421.3(154.0)	509.0(182.7)	32.8(1.0)	62.7(9.0)
Trot1	Go1	60.5(2.0)	88.9(6.5)	42.5(5.8)	20.0(10.2)
	A1	60.4(6.8)	97.5(8.1)	31.7(6.3)	21.5(2.2)
	AlienGo	150.9(80.2)	333.4(83.2)	31.9(2.9)	65.6(4.6)
Pace0	Go1	180.0(34.6)	176.1(21.9)	215.0(123.5)	21.4(3.3)
	A1	182.0(60.8)	212.3(28.9)	37.9(8.4)	41.7(31.7)
	AlienGo	385.4(157.2)	205.4(62.6)	31.3(2.2)	28.5(4.5)
Pace1	Go1	128.2(85.2)	601.1(137.3)	42.0(3.7)	36.1(2.4)
	A1	37.3(4.1)	330.7(128.3)	44.7(3.3)	75.3(0.4)
	AlienGo	159.6(92.0)	417.2(207.8)	37.8(2.2)	26.4(4.3)
SideSteps	Go1	148.6(21.7)	238.7(228.6)	171.2(30.4)	69.9(12.9)
	A1	224.6(60.1)	165.8(120.4)	200.3(29.2)	72.2(17.8)
	AlienGo	146.3(13.2)	276.2(115.3)	112.8(18.7)	69.1(12.1)
HopTurn	Go1	174.6(33.1)	212.8(5.2)	214.0(9.6)	57.9(5.9)
	A1	200.3(36.4)	297.3(128.2)	161.6(31.1)	40.6(5.1)
	AlienGo	154.3(54.6)	250.8(19.8)	73.8(10.6)	54.6(6.9)

Table 2: Keypoint L1 distance with Dynamic time warping (mm). Average values are listed with standard deviations in parentheses.

learning. However, our method also refines the motion in the temporal dimension. To evaluate the effects of temporal optimization, we compare the tracking performance with OptMimic, which utilizes contact-implicit trajectory optimization to refine a reference trajectory.

6.3. Motion Retargeting with diverse motion sets

We compare the proposed method and baselines in terms of the tracking performance by measuring the distance between keypoints of reference trajectory and deployed motion. In particular, we utilize Dynamic time warping (DTW) (Senin, 2008) to measure distance irrelevant to temporal deformation, avoiding the risk of under-evaluating baseline methods.

We evaluate the tracking error across motions of varying complexity from the work of Smith et al. (2022). Regarding the complexity of these motions, they can be ranked in ascending order as follows: Trot, Pace, SideSteps, and HopTurn. Trot motion is comparatively more straightforward to replicate than Pace as it involves cross-arranging two feet for enhanced stability. Both Pace and SideSteps involve statically unstable postures. However, SideSteps

Motion	Robot	DeepMimic	AMP	OptMimic	STMR (ours)
SideSteps	Go1	4.0(0.6)	6.4(6.1)	3.5(0.6)	1.9(0.3)
	A1	7.2(1.9)	5.3(3.8)	5.0(0.7)	2.7(0.7)
	AlienGo	3.7(0.3)	6.9(2.9)	2.7(0.4)	1.7(0.3)
HopTurn	Go1	6.5(1.2)	7.9(0.2)	6.1(0.3)	2.1(0.2)
	A1	8.2(1.5)	12.2(5.2)	4.4(0.8)	1.6(0.2)
	AlienGo	5.3(1.9)	8.5(0.7)	2.1(0.3)	1.7(0.2)

Table 3: Normalized Keypoint L1 distance with Dynamic time warping (%). Average values are listed with standard deviations in parentheses.

poses a greater challenge due to the need to balance against lateral momentum. Lastly, HopTurn is the most complex, as it requires jumping and a mid-air maneuver of turning. In terms of the target robot, we employ three different sizes of quadrupedal robots (Unitree A1, Unitree Go1, and Unitree AlienGo). In addition, we elongated the length of each motion with a scale of two, which roughly corresponds to obtaining motion with larger configurations.

The tracking performance in terms of mean and standard deviation over 5 random seeds is summarized in Table 2. The result shows that the STMR method exhibits exceptional performance across all six motions, with an average tracking error of 48.7 mm. In comparison, the average errors for the three baseline methods—DeepMimic, AMP, and OptMimic—are 168.3 mm, 275.3 mm, and 88.4 mm, respectively. Thus, the improvement in tracking error achieved by our method corresponds to 71.0%, 82.3%, and 44.86% reductions for each of the baseline methods. We also report tracking errors normalized by the total length of the keypoint trajectories as Table 3. The result shows that STMR’s tracking performance stands out, particularly for the two most challenging motions (i.e., SideSteps and HopTurn), surpassing three baselines by an average of 3.93%, whereas STMR’s average error is 1.95%.

6.4. Foot slide regularization and contact schedule preservation

SMR enforces foot constraints to generate kinematically feasible motions that preserve the original contact schedules and avoid foot sliding. Therefore, we quantitatively evaluate foot sliding and contact preservation using the same six motions from the previous Section 6.3. We measure foot sliding by calculating the L1 distance of position between the beginning and end

Robot	Motion	Foot slide ↓		IoU ↑	
		UV	Ours	UV	Ours
Go1	Trot0	110.19	0.15	0.46	1.00
	Trot1	72.93	0.09	0.48	1.00
	Pace0	88.90	0.14	0.47	1.00
	Pace1	61.33	0.09	0.53	0.99
	SideSteps	34.74	0.03	0.6	1.00
	HopTurn	33.35	0.05	0.59	1.00
A1	Trot0	101.39	0.15	0.44	1.00
	Trot1	86.29	0.12	0.5	1.00
	Pace0	83.29	0.12	0.47	1.00
	Pace1	63.58	0.11	0.53	1.00
	SideSteps	41.37	0.04	0.58	1.00
	HopTurn	37.19	0.05	0.49	1.00
AlienGo	Trot0	147.01	0.07	0.46	1.00
	Trot1	112.22	2.89	0.54	0.98
	Pace0	114.51	0.10	0.49	1.00
	Pace1	71.88	0.09	0.53	1.00
	SideSteps	26.34	0.04	0.5	1.00
	HopTurn	44.11	1.83	0.58	1.00

Table 4: Evaluation of foot slide and contact preservation. Foot slide, measured in mm/s, denotes the displacement rate of the foot during motion. Contact preservation signifies the degree of overlap between the transferred and ground truth contact boolean, and it is evaluated using intersection over union (IoU). The symbol \uparrow means higher values indicate better performance, while \downarrow suggests lower values represent superior performance.

of the contact segment, where continuous contact longer than 0.5 second is marked as the contact segment. Additionally, we measure the contact preservation through the Intersection over Union (IoU) between the contact schedules of the original and retargeted motion. An IoU of 1.0 between two motions signifies identical contact schedules, indicating successful contact preservation, whereas an IoU of 0.0 indicates completely divergent contact schedules.

To evaluate foot slide regularization and contact preservation, we compare against the unit vector method as the baseline method, where the results are summarized in Table 4. The proposed method shows an average foot sliding of 0.34mm, whereas that of the baseline method is 73.92mm across six motions and three robots. Furthermore, the proposed method also shows significant improvement in contact preservation, with an average IoU of 0.998 compared to 0.513 for the baseline method. Given that the foot sliding error

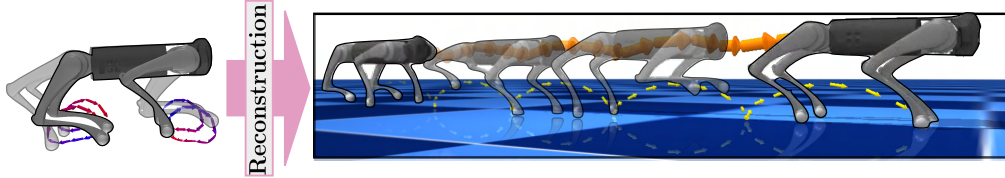


Figure 5: Reconstruction of base movement from keypoint trajectory

and the IoU achieve near-optimal values, the results strongly suggest that the motions generated by our method effectively eliminate foot sliding and accurately preserve contact schedules.

6.5. Motion retargeting from baseless motion

The proposed method generates the whole-body motion from the baseless keypoint trajectories. Therefore, we evaluate its capability by removing and reconstructing the base movement, subsequently measuring the reconstruction error. Leveraging the reconstructing capability, we demonstrate motion retargeting with the keypoint trajectories obtained from video pose estimation.

6.5.1. Reconstruction of whole-body motion

Figure 5 shows the overview of reconstructing a whole-body motion. As shown in the left side of Figure 5, we remove the base position \mathbf{p}_b from whole-body motion, leaving only the keypoint trajectories $\mathbf{p}_{1:N}^{0:T}$. We then reconstruct the base position \mathbf{p}_b , as shown on the right side of Figure 5. The reconstruction is performed with different gait patterns and velocities: Pace (1.0m/s), Bound (1.0m/s), and Trot (0.5 m/s, 1.0 m/s, 1.5m/s), which are synthesized using model-based optimal control (MBOC) (Tassa et al., 2012).

We measure the positional difference with respect to the ground-truth data, which is motions before clearing the base position. In detail, we measure the positional error in L1 distance per frame and divide it by the distance base point traveled. The resulting errors of reconstruction for pacing, bounding, and three trotting motions are 12.71%, 11.66%, 10.81%, 11.51%, and 14.31%, respectively. The average reconstruction error of 12.188% shows the proposed method can generate whole-body motion from baseless motion.

6.5.2. Motion retargeting from videos

Leveraging the reconstruction capability of the proposed method, we demonstrate motion retargeting with keypoint trajectories obtained from the

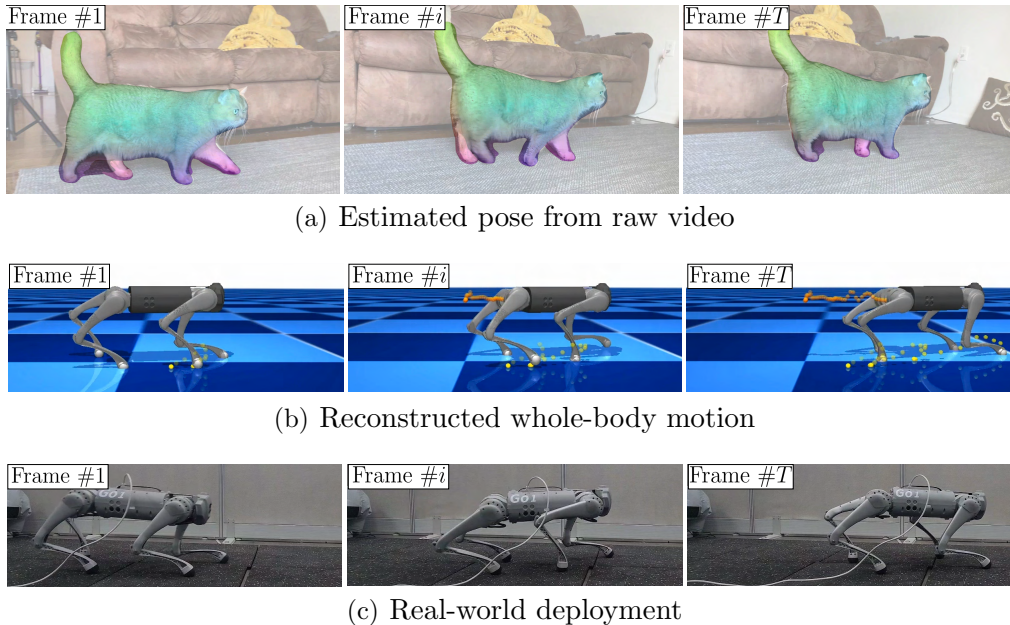


Figure 6: The keypoint trajectories are extracted using pose-estimator (Yang et al., 2022) and reconstructed as a whole-body motion. Subsequently, the motion is utilized as a reference motion to train control policy for real-world deployment.

video pose estimator (Yang et al., 2022). Although we utilize the pose estimator, which provides the base position, its estimation is noisy because the absolute position of the camera is unknown. Therefore, we remove and reconstruct the base position to obtain kinematically feasible whole-body motion. Subsequently, we temporally optimize the kinematic motion to consider the dynamic properties of the robot. Finally, we train residual policy as in Section 6.3, where the resulting motion is illustrated in Figure 6.

7. Real-world Experiments

We demonstrate that the learned policies can successfully imitate the target motions in a real-world environment using two robots: Go1 (Unitree) and AlienGo (Unitree). As illustrated in Figure 7, the control policy runs at 50Hz, successfully responding in real-time to execute the dynamic motion of HopTurn and SideSteps on two robots, overcoming the difference in kinematic

and dynamic properties¹. We emphasize that the HopTurn motion refined by our STMR method features physically coherent mid-air time. Additionally, the refined SideSteps motion results in stable horizontal movements. We note that we only executed the motions generated by our method on the hardware because deploying other baseline methods could likely damage the robots.

To overcome the innate uncertainty of the real-world environment, we use domain randomization (Zhao et al., 2020) to randomize controller gains, mass, inertia, friction, and floor restitution and randomly push the robot to change to torso velocity, where the randomization ranges are summarized in Table 5. In addition, estimating the base height (Bloesch et al., 2013) and incorporating it into the state contributed to reducing the sim-to-real gaps, especially for jumping motion in HopTurn.

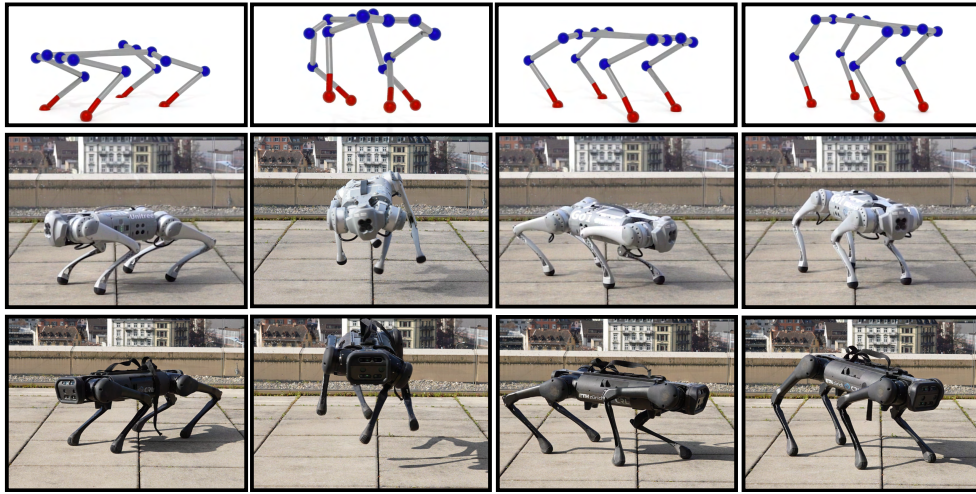
Values	Minimum	Maximum
Friction	0.75	1.00
Mass(kg)	-1.0	1.0
Proportional Gain Multiplier	0.9	1.1
Damping Gain Multiplier	0.9	1.1
Restitution	0.0	0.5
COM displacement (mm)	-100	100

Table 5: Sampling ranges for domain randomization.

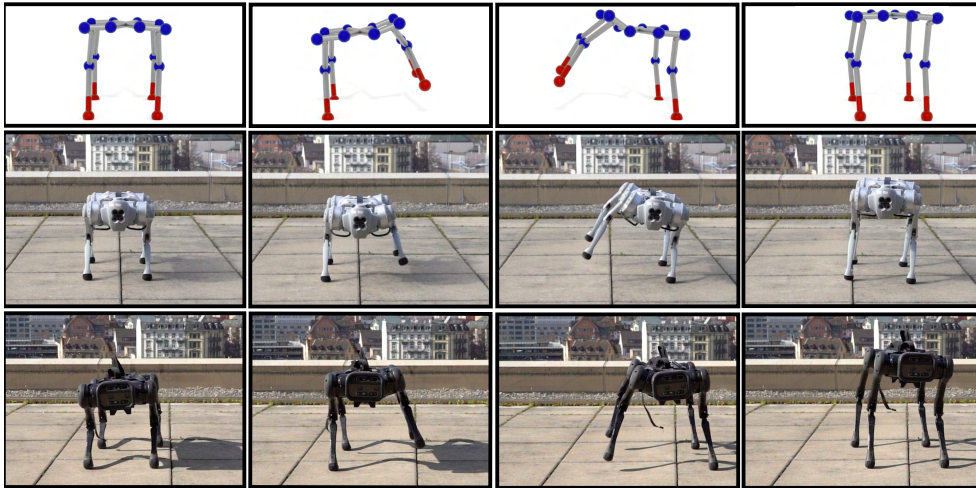
8. Limitation

The proposed method involves generating whole-body motion from baseless motion by utilizing the contact sequence. However, this process heavily relies on accurate contact estimation, whereas wrong estimation can cause irregular movements that propagate during the construction of whole-body motions. In particular, the estimated contact phase can change discontinuously as we obtain the contact boolean by thresholding the foot’s velocity. This can lead to jerky motions or failure of imitation, as robots can not follow such a quick contact transition. In our experiments, we partially overcome this problem by applying a low-pass filter, which regularizes high-frequency change of contact phases.

¹The footage from the experiments can be found in the attached video.



(a) HopTurn



(b) SideSteps

Figure 7: Deployment of control policy in real-world.

9. Conclusion

This paper introduces the problem of spatio-temporal motion retargeting (STMR) that aims to generate physically feasible motion to guide the imitation learning process. The STMR ensures that the transferred motions are kino-dynamically feasible for the target system. Furthermore, it facilitates the use of motion data with the unknown origin of reference by generat-

ing whole-body motions that closely mimic the agility and expressiveness of natural animal movements.

Our comprehensive experiments demonstrate STMR’s superiority in control policy learning, which facilitates more accurate and dynamic motion imitation than baseline methods. We further evaluate the elimination of foot sliding and the preservation of contact schedules of the resulting motions. The successful deployment of these motions in real-world scenarios highlights the practical applicability of STMR in enhancing control policy learning for quadrupeds.

Our proposed method relies on accurate contact estimation. In future work, we aim to enhance this approach to be more robust against noise in contact schedules.

Acknowledgement

This work was supported by the Institute of Information & Communications Technology Planning & Evaluation (IITP) grant funded by the Korea government (MSIT). The contributions from the Institute of Information & Communications Technology Planning & Evaluation (IITP) were funded by four separate grants: No. 2019-0-00079, Artificial Intelligence Graduate School Program (Korea University), No. 2022-0-00871, Development of AI Autonomy and Knowledge Enhancement for AI Agent, No. 2022-0-00480, Development of Training and Inference Methods for Goal-Oriented Artificial Intelligence Agents, and No. 2022-0-00612, Geometric and Physical Commonsense Reasoning based Behavior Intelligence for Embodied AI.

The authors thank Jin Cheng for his assistance with the experiments.

References

- Aberman, K., Li, P., Lischinski, D., Sorkine-Hornung, O., Cohen-Or, D., Chen, B., 2020. Skeleton-aware networks for deep motion retargeting. *ACM Transactions on Graphics* 39. URL: <https://dl.acm.org/doi/10.1145/3386569.3392462>, doi:10.1145/3386569.3392462.
- Al Borno, M., Righetti, L., Black, M.J., Delp, S.L., Fiume, E., Romero, J., 2018. Robust Physics-based Motion Retargeting with Realistic Body Shapes. *Computer Graphics Forum* 37, 81–92. URL: <https://onlinelibrary.wiley.com/doi/10.1111/cgf.13514>, doi:10.1111/cgf.13514.

- Bloesch, M., Hutter, M., Hoepflinger, M.A., Leutenegger, S., Gehring, C., Remy, C.D., Siegwart, R., 2013. State estimation for legged robots: Consistent fusion of leg kinematics and imu .
- Chiaverini, S., Siciliano, B., Egeland, O., 1994. Review of the damped least-squares inverse kinematics with experiments on an industrial robot manipulator. *IEEE Transactions on Control Systems Technology* 2, 123–134. URL: <http://ieeexplore.ieee.org/document/294335/>, doi:10.1109/87.294335.
- Choi, S., Kim, J., 2019. Towards a natural motion generator: a pipeline to control a humanoid based on motion data, in: 2019 IEEE/RSJ International Conference on Intelligent Robots and Systems (IROS), pp. 4373–4380. doi:10.1109/IROS40897.2019.8967941.
- Choi, S., Pan, M., Kim, J., 2020. Nonparametric motion retargeting for humanoid robots on shared latent space, in: 16th Robotics: Science and Systems, RSS 2020, MIT Press Journals.
- Choi, S., Song, M.J., Ahn, H., Kim, J., 2021. Self-Supervised Motion Retargeting with Safety Guarantee, in: 2021 IEEE International Conference on Robotics and Automation (ICRA), IEEE, Xi'an, China. pp. 8097–8103. URL: <https://ieeexplore.ieee.org/document/9560860/>, doi:10.1109/ICRA48506.2021.9560860.
- Devin, C., Gupta, A., Darrell, T., Abbeel, P., Levine, S., 2017. Learning modular neural network policies for multi-task and multi-robot transfer, in: 2017 IEEE international conference on robotics and automation (ICRA), IEEE. pp. 2169–2176.
- Escontrela, A., Peng, X.B., Yu, W., Zhang, T., Iscen, A., Goldberg, K., Abbeel, P., 2022. Adversarial Motion Priors Make Good Substitutes for Complex Reward Functions, in: 2022 IEEE/RSJ International Conference on Intelligent Robots and Systems (IROS), IEEE, Kyoto, Japan. pp. 25–32. URL: <https://ieeexplore.ieee.org/document/9981973/>, doi:10.1109/IROS47612.2022.9981973.
- Feng, G., Zhang, H., Li, Z., Peng, X.B., Basireddy, B., Yue, L., Song, Z., Yang, L., Liu, Y., Sreenath, K., et al., 2023. Genloco: Generalized locomotion controllers for quadrupedal robots, in: Conference on Robot Learning, PMLR. pp. 1893–1903.

- Fuchioka, Y., Xie, Z., Van De Panne, M., 2023. OPT-Mimic: Imitation of Optimized Trajectories for Dynamic Quadruped Behaviors, in: 2023 IEEE International Conference on Robotics and Automation (ICRA), IEEE, London, United Kingdom. pp. 5092–5098. URL: <https://ieeexplore.ieee.org/document/10160562/>, doi:10.1109/ICRA48891.2023.10160562.
- Grandia, R., Farshidian, F., Knoop, E., Schumacher, C., Hutter, M., Bächer, M., 2023. DOC: Differentiable Optimal Control for Retargeting Motions onto Legged Robots. *ACM Transactions on Graphics* 42, 1–14. URL: <https://dl.acm.org/doi/10.1145/3592454>, doi:10.1145/3592454.
- Gu, S., Zhu, F., 2024. Bagail: Multi-modal imitation learning from imbalanced demonstrations. *Neural Networks* , 106251.
- Johannink, T., Bahl, S., Nair, A., Luo, J., Kumar, A., Loskyll, M., Ojea, J.A., Solowjow, E., Levine, S., 2019. Residual reinforcement learning for robot control, in: 2019 International Conference on Robotics and Automation (ICRA), pp. 6023–6029. doi:10.1109/ICRA.2019.8794127.
- Kang, D., Cheng, J., Zamora, M., Zargarbashi, F., Coros, S., 2023. RL + Model-Based Control: Using On-Demand Optimal Control to Learn Versatile Legged Locomotion. *IEEE Robotics and Automation Letters* 8, 6619–6626. URL: <https://ieeexplore.ieee.org/document/10225268/>, doi:10.1109/LRA.2023.3307008.
- Kang, D., De Vincenti, F., Adami, N.C., Coros, S., 2022. Animal Motions on Legged Robots Using Nonlinear Model Predictive Control, in: 2022 IEEE/RSJ International Conference on Intelligent Robots and Systems (IROS), IEEE, Kyoto, Japan. pp. 11955–11962. URL: <https://ieeexplore.ieee.org/document/9981945/>, doi:10.1109/IROS47612.2022.9981945.
- Kang, D., Zimmermann, S., Coros, S., 2021. Animal Gaits on Quadrupedal Robots Using Motion Matching and Model-Based Control, in: 2021 IEEE/RSJ International Conference on Intelligent Robots and Systems (IROS), IEEE, Prague, Czech Republic. pp. 8500–8507. URL: <https://ieeexplore.ieee.org/document/9635838/>, doi:10.1109/IROS51168.2021.9635838.

- Kim, S., Sorokin, M., Lee, J., Ha, S., 2022. HumanConQuad: Human Motion Control of Quadrupedal Robots using Deep Reinforcement Learning, in: SIGGRAPH Asia 2022 Emerging Technologies, ACM, Daegu Republic of Korea. pp. 1–2. URL: <https://dl.acm.org/doi/10.1145/3550471.3564762>, doi:10.1145/3550471.3564762.
- Kingma, D.P., Ba, J., 2014. Adam: A method for stochastic optimization. arXiv preprint arXiv:1412.6980 .
- Kwang-Jin Choi, Hyeong-Seok Ko, 1999. On-line motion retargetting, in: Proceedings. Seventh Pacific Conference on Computer Graphics and Applications (Cat. No.PR00293), IEEE Comput. Soc, Seoul, South Korea. pp. 32–42. URL: <http://ieeexplore.ieee.org/document/803346/>, doi:10.1109/PCCGA.1999.803346.
- Levine, S., Koltun, V., 2013. Guided policy search, in: International conference on machine learning, PMLR. pp. 1–9.
- Li, C., Vlastelica, M., Blaes, S., Frey, J., Grimminger, F., Martius, G., 2023a. Learning agile skills via adversarial imitation of rough partial demonstrations, in: Conference on Robot Learning, PMLR. pp. 342–352.
- Li, T., Won, J., Clegg, A., Kim, J., Rai, A., Ha, S., 2023b. Ace: Adversarial correspondence embedding for cross morphology motion retargeting from human to nonhuman characters, in: SIGGRAPH Asia 2023 Conference Papers, Association for Computing Machinery, New York, NY, USA. URL: <https://doi.org/10.1145/3610548.3618255>, doi:10.1145/3610548.3618255.
- Makoviychuk, V., Wawrzyniak, L., Guo, Y., Lu, M., Storey, K., Macklin, M., Hoeller, D., Rudin, N., Allshire, A., Handa, A., et al., 2021. Isaac gym: High performance gpu-based physics simulation for robot learning. arXiv preprint arXiv:2108.10470 .
- Mayne, D.Q., 1973. Differential Dynamic Programming—A Unified Approach to the Optimization of Dynamic Systems* *This work was done during the author’s visit to the Division of Engineering and Applied Physics, Harvard University, and was supported by the U.S. Army Research Office, the U.S. Air Force Office of Scientific Research and the U.S. Office of Naval Research under the Joint Services

- Electronics Program by Contracts N00014-67-A-0298-0006, 0005. and 0008., in: Control and Dynamic Systems. Elsevier. volume 10, pp. 179–254. URL: <https://linkinghub.elsevier.com/retrieve/pii/B9780120127108500108>, doi:10.1016/B978-0-12-012710-8.50010-8.
- Mayr, M., Ahmad, F., Duerr, A., Krueger, V., 2023. Using knowledge representation and task planning for robot-agnostic skills on the example of contact-rich wiping tasks, in: 2023 IEEE 19th International Conference on Automation Science and Engineering (CASE), IEEE. pp. 1–7.
- Nakamura, Y., Mori, T., Sato, M.a., Ishii, S., 2007. Reinforcement learning for a biped robot based on a cpg-actor-critic method. *Neural networks* 20, 723–735.
- Oh, H., Sasaki, H., Michael, B., Matsubara, T., 2023. Bayesian disturbance injection: Robust imitation learning of flexible policies for robot manipulation. *Neural Networks* 158, 42–58.
- Peng, X.B., Abbeel, P., Levine, S., Van De Panne, M., 2018. DeepMimic: example-guided deep reinforcement learning of physics-based character skills. *ACM Transactions on Graphics* 37, 1–14. URL: <https://dl.acm.org/doi/10.1145/3197517.3201311>, doi:10.1145/3197517.3201311.
- Peng, X.B., Coumans, E., Zhang, T., Lee, T.W.E., Tan, J., Levine, S., 2020. Learning agile robotic locomotion skills by imitating animals, in: *Robotics: Science and Systems*. doi:10.15607/RSS.2020.XVI.064.
- Peng, X.B., Ma, Z., Abbeel, P., Levine, S., Kanazawa, A., 2021. AMP: adversarial motion priors for stylized physics-based character control. *ACM Transactions on Graphics* 40, 1–20. URL: <https://dl.acm.org/doi/10.1145/3450626.3459670>, doi:10.1145/3450626.3459670.
- Rouxel, Q., Yuan, K., Wen, R., Li, Z., 2022. Multicontact Motion Retargeting Using Whole-Body Optimization of Full Kinematics and Sequential Force Equilibrium. *IEEE/ASME Transactions on Mechatronics* 27, 4188–4198. URL: <https://ieeexplore.ieee.org/document/9728754/>, doi:10.1109/TMECH.2022.3152844.
- Schulman, J., Wolski, F., Dhariwal, P., Radford, A., Klimov, O., 2017. Proximal policy optimization algorithms. arXiv preprint arXiv:1707.06347 .

- Senin, P., 2008. Dynamic time warping algorithm review. Information and Computer Science Department University of Hawaii at Manoa Honolulu, USA 855, 40.
- Seol, Y., O’Sullivan, C., Lee, J., 2013. Creature features: online motion puppetry for non-human characters, in: Proceedings of the 12th ACM SIGGRAPH/Eurographics Symposium on Computer Animation, ACM, Anaheim California. pp. 213–221. URL: <https://dl.acm.org/doi/10.1145/2485895.2485903>, doi:10.1145/2485895.2485903.
- Shahbazi, H., Parandeh, R., Jamshidi, K., 2016. Implementation of imitation learning using natural learner central pattern generator neural networks. Neural Networks 83, 94–108.
- Smith, L., Kew, J.C., Peng, X.B., Ha, S., Tan, J., Levine, S., 2022. Legged robots that keep on learning: Fine-tuning locomotion policies in the real world, in: 2022 International Conference on Robotics and Automation (ICRA), IEEE. pp. 1593–1599.
- Snoek, J., Larochelle, H., Adams, R.P., 2012a. Practical bayesian optimization of machine learning algorithms. Advances in neural information processing systems 25.
- Snoek, J., Larochelle, H., Adams, R.P., 2012b. Practical bayesian optimization of machine learning algorithms, in: Pereira, F., Burges, C., Bottou, L., Weinberger, K. (Eds.), Advances in Neural Information Processing Systems, Curran Associates, Inc. URL: https://proceedings.neurips.cc/paper_files/paper/2012/file/05311655a15b75fab86956663e1819cd-Paper.pdf.
- Tak, S., Ko, H.S., 2005. A physically-based motion retargeting filter. ACM Transactions on Graphics 24, 98–117. URL: <https://dl.acm.org/doi/10.1145/1037957.1037963>, doi:10.1145/1037957.1037963.
- Tassa, Y., Erez, T., Todorov, E., 2012. Synthesis and stabilization of complex behaviors through online trajectory optimization, in: 2012 IEEE/RSJ International Conference on Intelligent Robots and Systems, IEEE, Vilamoura-Algarve, Portugal. pp. 4906–4913. URL: <http://ieeexplore.ieee.org/document/6386025/>, doi:10.1109/IRoS.2012.6386025.

- Villegas, R., Yang, J., Ceylan, D., Lee, H., 2018. Neural Kinematic Networks for Unsupervised Motion Retargetting, in: 2018 IEEE/CVF Conference on Computer Vision and Pattern Recognition, IEEE, Salt Lake City, UT. pp. 8639–8648. URL: <https://ieeexplore.ieee.org/document/8578999/>, doi:10.1109/CVPR.2018.00901.
- Yamane, K., Ariki, Y., Hodgins, J., 2010. Animating non-humanoid characters with human motion data, in: Proceedings of the 2010 ACM SIGGRAPH/Eurographics Symposium on Computer Animation, Eurographics Association, Goslar, DEU. p. 169–178.
- Yang, G., Vo, M., Neverova, N., Ramanan, D., Vedaldi, A., Joo, H., 2022. Banmo: Building animatable 3d neural models from many casual videos, in: 2022 IEEE/CVF Conference on Computer Vision and Pattern Recognition (CVPR), pp. 2853–2863. doi:10.1109/CVPR52688.2022.00288.
- Zhang, L., Liu, Q., Zhu, F., Huang, Z., 2023a. Addressing implicit bias in adversarial imitation learning with mutual information. *Neural Networks* 167, 847–864.
- Zhang, Y., Thor, M., Dilokthanakul, N., Dai, Z., Manoonpong, P., 2023b. Hybrid learning mechanisms under a neural control network for various walking speed generation of a quadruped robot. *Neural Networks* 167, 292–308.
- Zhao, W., Queralta, J.P., Westerlund, T., 2020. Sim-to-real transfer in deep reinforcement learning for robotics: a survey, in: 2020 IEEE symposium series on computational intelligence (SSCI), IEEE. pp. 737–744.
- Zhou, Y., Lu, M., Liu, X., Che, Z., Xu, Z., Tang, J., Zhang, Y., Peng, Y., Peng, Y., 2023. Distributional generative adversarial imitation learning with reproducing kernel generalization. *Neural Networks* 165, 43–59.